International Journal of Emerging Technology and Advanced Engineering
Website: www.ijetae.com (ISSN 2250-2459, ISO 9001:2008 Certified Journal, Volume 7, Issue 8, August 2017)

Conceptual Design, Analysis and Optimization of Unmanned Aerial Vehicle

Tejas Vishweshwara P[1], Suhas A Kedilaya[2], Ram Rohit Vannarth[3], Dr. Kayala Mallikharjuna Babu[4]
[1]*B.E, Student,* [2] *B.E Student,* [3]*Assistant Professor,* [4]*Principal, B.M.S College of Engineering, Bengaluru, India*

***Abstract*— This paper provides in-depth insight into the modern methods adopted to design, analyze & build an efficient radio controlled model of a plane. The UAV discussed in this paper can carry a payload fraction of 0.65 and has a self-weight of 0.5kg. Optimization of the plane is carried out by using simulation tools such as CATIA, ANSYS STRUCTURAL, FLUENT, XFLR. Balsa wood is predominantly employed for manufacturing process. The important parameters taken into consideration for the calculation purposes are highlighted. The analytical approach is discussed in detail for the design of Unmanned aerial vehicle (UAV).**

***Keywords*—Airfoil, Drag analysis, Fuselage, Stability, Tail sizing, Unmanned aerial vehicle (UAV).**

I. INTRODUCTION

The main aim of this paper is to showcase the detailed approach adopted in building a prototype of a radio-controlled plane capable of carrying heavy payload. The main application of such a plane design is in transporting medicines and goods to remote areas. The plane design and construction is made robust to protect the payload during landing and mid-flight turbulence.

The typical approach therefore is to design a plane with high payload fraction by making suitable air-frame modifications. Also the focus is on reducing the power requirement by not compromising on thrust to weight ratio. Various lift augmenting devices are used in the process of building the plane. The following are the various steps in the process.

- Payload and empty weight of the plane considering weight of electronics.
- Conduct a FOM study to identify suitable airplane configuration.
- Preliminary design by selecting a suitable airfoil.
- Carry out analysis and identify critical stress points.
- Optimize the design to reduce the stress. Reiterate the process.
- Carry out analysis to visualize the flow around wing and determine the coefficient of lift.
- Fabricate the prototype.
- Test and proceed for final construction.

II. DESIGN APPROACH

A. Configuration Selection

The best possible configuration can be obtained by comparing them over a range of design parameters as shown in Table I. This process is known as figure of merit.

TABLE I
FOM STUDY

Parameters	Conventional	Bi-plane	Boom wing
Lift Capacity	3.5	4	4
Stability	4	4	3
Construction	4	2.5	4
Weight	4	3.5	4
Cost	4	3	3

In the case of biplane design, payload bay cannot be mounted with ease and the resulting drag is high. Further the weight is also significantly more than a conventional design. For a boom wing design structural stability comes as a major drawback when the plane crashes. Further stability in turbulence condition poses serious challenges. A conventional design on the other hand is more stable and robust in design and fabrication and is hence a more suitable configuration.

B. Airfoil Selection

The airfoil shape influences C_{Lmax}, C_{Dmin} and stall pattern [1]. These in turn influence stalling speed & weight of the plane. Various airfoils are tested by using analysis software XFLR5. Airfoils E423, NACA 2412, s1223 & flat-bottomed s7055 [2] are tested for a Reynolds number of 100,000. It can be noted that s1223 has a superior aerodynamic performance when compared to other airfoils as indicated in Figure 1, but poses greater challenges in fabrication due to high camber.

International Journal of Emerging Technology and Advanced Engineering
Website: www.ijetae.com (ISSN 2250-2459, ISO 9001:2008 Certified Journal, Volume 7, Issue 8, August 2017)

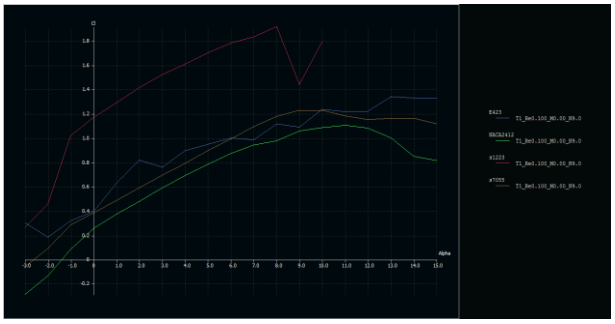

Figure 1: C_L vs. angle of attack

NACA 2412 airfoil is thicker than other airfoils and hence adds up to extra weight. E423 airfoil is of medium camber and shows promising result in terms of wing efficiency. The negative moment coefficient for E423 airfoil is larger than s1223 which reduces the torsion stress on the main spar of the wing frame design. Therefore E423 airfoil is selected for the aircraft wing. The small amount of waviness in the graphs is due to numerical instabilities and convergence errors at low Reynolds numbers.

C. Planform Selection

The lift force created by an arbitrary shaped object depends on the density of the surrounding medium, relative velocity of airflow and circulation around the object as established by Kutta-Joukowski theorem. It acts along centre of pressure. For a cambered airfoil, the circulation is a function of wing area, lift coefficient and angle of attack.

$$L = \rho_\infty V \Gamma$$

Or

$$L = 0.5\, \rho_\infty C_L A V^2$$

where,

ρ_∞ – *Density of air* V – *Relative free stream velocity*
C_L – *Coefficient of lift* Γ – *Circulation*

For a total weight of 1.5kg, initial incident angle of 6degrees, and considering the external flying conditions, above formulae yields wing area of 0.18m^2. Considering an aspect ratio of 8, span of wing is chosen to be 1.2m and chord length is 0.15m.

D. Lift Coefficient 3-D

A finite wing is a three dimensional body, and as a result there is a component of airflow in the spanwise direction. This occurs due to leakage around wing tips due to difference in pressure between top and bottom surface of airfoil. This leak effect establishes a circulatory motion called vortices.

The effect of vortices results in a downward component of air velocity at wing trailing edge. Thus the effective angle of attack differs from geometric angle of attack as shown in Figure 2.

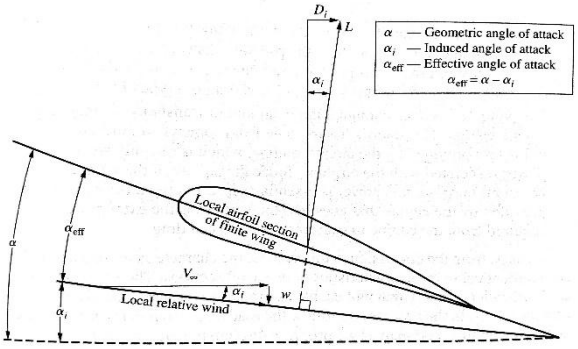

Figure 2: Effect of downwash on a finite wing [3].

The finite wing lift curve has the same zero lift angle of attack, and pivots about this point, clockwise. The reduced slope $dC_l/d\propto$ derived from theory is given by,

$$\frac{dC_l}{d\alpha} = \frac{2\pi * (AR)}{2 + \left[4 + (AR \times \beta)^2 \left(1 + \frac{tan^2(\Lambda)}{\beta^2}\right)\right]^{1/2}}$$

where,

$$\beta = (1 - M_{eff}^2)^{1/2}$$

$$M_{eff} = M_\infty \cos(\Lambda)$$

$$C_L = \frac{dC_L}{d\alpha}\,(\alpha - \alpha_{eff})$$

AR – Aspect ratio of the wing
M_∞ – *Free stream Mach number*
M_{eff} – *Effective Mach number*
Λ – *Sweep angle of the wing*

The value of $\frac{dC_l}{d\alpha}$ obtained from the numerical result is 0.087. The angle of attack corresponding to zero lift coefficient is -4^0. This yields finite wing lift coefficient equal to 0.87 at incident angle of attack of 6^0.

E. Horizontal Tail Design

The horizontal tail design is made flat. The reason for the corresponding choice is as follows.

International Journal of Emerging Technology and Advanced Engineering
Website: www.ijetae.com (ISSN 2250-2459, ISO 9001:2008 Certified Journal, Volume 7, Issue 8, August 2017)

A symmetric airfoil design produces significant amount of drag based on airfoil thickness and causes weight penalty. Alternately, a cambered airfoil can lead to added complexity of manufacturing process despite increase in lift. Hence it is decided to incorporate a flat plate design owing to the ease of manufacturing, significant reduction in weight, drag of the tail assembly and moderate amount of lift. The volume coefficient is given by,

$$V_h = \frac{l_h S_h}{S_w \bar{c}}$$

V_h – *Tail Co-efficient*
S_w – *Area of wing*
S_h – *Area of Horizontal tail*
l_h – *Distance from center of gravity to aerodynamic center of horizontal tail*
$\bar{c}$ – *Mean aerodynamic chord*

The volume coefficient which is the deciding factor for area of horizontal tail is fixed at 0.5 considering the database. This ensures a low permissible travel of center of gravity. The area of horizontal tail is equal to 0.036m^2. Hence the width and length of tail is chosen as

Span	400mm
Width	90mm

F. Vertical tail design

The vertical tail volume co-efficient is given by,

$$V_v = \frac{l_v S_v}{S_w b}$$

V_v – *Tail Co-efficient*
S_w – *Area of wing*
S_v – *Area of Horizontal tail*
l_v – *Distance from center of gravity to aerodynamic center of vertical tail*
b – *Span*

A volume coefficient equal to 0.03 is chosen for vertical tail design. The area of vertical tail is equal to 0.0135m^2. Hence the width and length of tail is chosen as

Span	150mm
Width	90mm

III. Analysis & Optimization

A. Thrust Analysis

The thrust force counters the drag force and enables the forward motion of the plane. The magnitude of thrust is dependent on the amount of air that is pushed backward and its corresponding velocity. The major thrust component in an RC plane are motors and propellers. The motor generates certain RPM which is exerted on air by suitable size propeller. The selection of motor depends on the type of propeller chosen. The power required at different flight velocities is calculated by,

$$P_{req} = \frac{1}{2}\rho V^3 S C_{D0} + \frac{W^2}{\frac{1}{2}\rho V S}\left(\frac{1}{\pi e AR}\right)$$

The power required is calculated along the range of velocities of 1m/s to 20m/s. Drag factors are taken into account. Figure 3 shows the power required as a function of flight velocity. Power required at low velocity is more due to the lift induced drag at low speeds. As the speed increases, power required decreases until a particular velocity is attained after which the power required again increases due to parasitic drag at higher speeds. Based on the minimum power requirements, a suitable motor is selected.

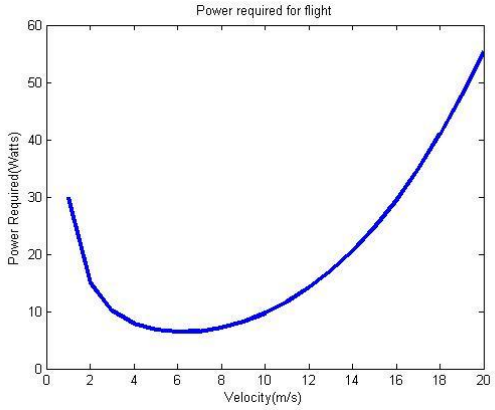

Figure 3: Power variation with velocity plotted using MATLAB.

The primary equation considered in motor selection is the relationship between the motor thrust and the RPM given by,

$$RPM = K_V \times V_{battery}$$

$V_{battery}$ – *Voltage delivered by battery*
K_V – *RPM per volt*

International Journal of Emerging Technology and Advanced Engineering
Website: www.ijetae.com (ISSN 2250-2459, ISO 9001:2008 Certified Journal, Volume 7, Issue 8, August 2017)

With decrease in the value of K_V the RPM of the motor decreases but gives more torque. The choice of suitable motor is made by taking into account numerous constraints such as

- Amount of current required to power the motor.
- Weight of the setup.
- RPM of motor.

A brushless out runner motor of 1200 K_V is selected which has the required power to propel the aircraft. For the selection of propeller, a database is generated by sorting the propellers by their pitch to diameter ratio (*P/D*). From the database, four different propeller sizes were selected and thrust provided by these propellers is tested for the selected motor using thrust meter. Based on this analysis, an optimum propeller of 10x5 is chosen.

TABLE II
PROPELLER SIZING

Propeller size	Thrust (grams)
10x5	1200
11x7	1150
9x7	1000
9x6	900

The thrust provided by the selected motor is calculated theoretically which is given by,

$$V_{pitch} = RPM \times pitch \times \eta_{propeller}$$

Where $\eta_{propeller}$ is the efficiency of propeller which is taken as 0.7

$$Thurst = \frac{Power}{V_{pitch}}$$

V_{pitch} is obtained as 20m/s. The thrust is obtained as 12.5N. Therefore the thrust provided by motor is 1270grams. Thus the thrust to weight ratio for loaded case is 0.84. The analytical result obtained above is comparable to the experimental result indicated in Table II.

B. Servo Sizing

The flight control is achieved by control surfaces mounted at specific points on the plane. These control surfaces such as ailerons, rudder & elevator are actuated using the servo motors.

These control surfaces are subjected to varying loads and hence need high torque servos to achieve the purpose. Also the degree of rotation is crucial to adjust the sensitivity of these surfaces. This is controlled by using clevises & connecting rod. Considering the maximum velocity attained to be 10-12m/s, the force exerted on control surface is calculated as torques on each servos.

$$Torque = 0.61206 \frac{c^2\, v^2\, L\, sin(s1)\, tan(s1)}{tan(s2)}$$

where,
c –*control surface chord in cm.*
L–control surface length in cm.
v – Speed in cm/s.
s1 – maximum control surface deflection in degrees.
s2 – maximum servo deflection in degrees.

Ailerons – 0.3 kg-cm	Elevators – 0.52 kg-cm	Rudder – 0.19 kg-cm

Hence servos of torque equal to 1.3 kg-cm is chosen to actuate the control surfaces.

C. 3-D Drag Analysis

In this analysis, the total drag on the aircraft is estimated. The 3-D drag polar of the aircraft is approximated using equation,

$$C_D = C_{Do} + K'C_L^2 + K''(C_L - C_{Lmin})^2$$

C_{Do} *– Pressure and skin friction drag*
K' – Induced drag factor
$K'C_L^2$ *– Lift induced drag*
C_{Lmin} *– C_L for minimum wing drag*
K" – Viscous induced factor
$K''(C_L - C_{Lmin})^2$ *– Viscous drag due to lift*

Here both *K"* and C_{Lmin} are determined from airfoil data. C_{Do} is predominantly skin friction drag and is found by adding the contributions of each component as calculated by below equation

$$C_{Do} = \frac{FF \times C_f \times S_{wetted}}{S_{planform}}$$

FF *– Form factor*
S_{wetted} *– Wetted surface area*
C_f *– Skin friction coefficient*
$S_{planform}$ *–Planform area of the components*

International Journal of Emerging Technology and Advanced Engineering
Website: www.ijetae.com (ISSN 2250-2459, ISO 9001:2008 Certified Journal, Volume 7, Issue 8, August 2017)

In the above equation, *FF* represents pressure drag contribution which is derived from empirical formula.

The wetted area of the wing is approximated as,

$$S_{wetted} = S_{exposed}\left[1.977 + 0.52\left(\frac{t}{c}\right)\right] \quad if\ \frac{t}{c} > 0.05$$

Since the aircraft travels at speeds of 5-12m/s, the Reynolds number varies between 40,000 to 2,00,000 for that range considering a chord of 0.15m. For the following range, C_f is given by

$$C_f = \frac{1.328}{Re^{0.5}}$$

$Re -$ *Reynolds number*

TABLE III
CALCULATION OF C_{Do}

Parameters	Wing	Fuselage	Vertical Tail	Horizontal Tail
$S_{ref}(m^2)$	0.167	0.0321	0.0112	0.0312
$S_{wet}(m^2)$	0.342	0.1357	0.0228	0.0644
S_{wet}/S_{ref}	2.038	4.22	2.03	2.064
FF	1.323	1.148	1.025	1.025
C_f	0.003	0.00195	0.0043	0.0043
C_{Do}	0.010	0.00945	0.00895	0.00909
Total C_{Do}			0.03816	

Therefore C_{Do} is 0.03816 as derived in Table III. The induced drag factor ($K^{'}$) is given by,

$$K' = \frac{1}{\pi\, AR\, e}$$

$AR -$ *wing aspect ratio*
$e -$ *wingspan efficiency*

K', *AR* and *e* are calculated to be 0.042, 8 and 0.95 respectively. C_{Lmin} is determined for the point of lowest C_D from the drag polar as shown in Figure 4.

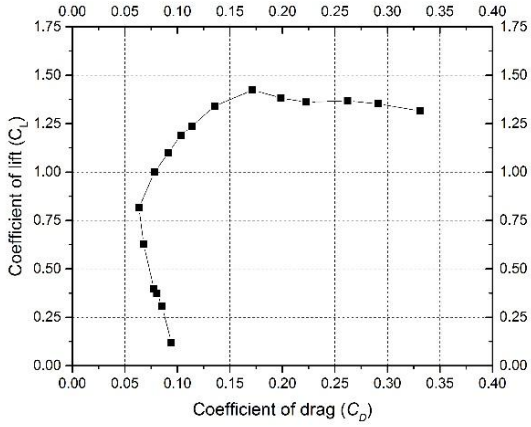

Figure 4: Drag Polar of airfoil.

Viscous induced drag factor *K''* is equal to 0.2286 determined by the slope of nearly linear relation as shown in Figure 5. C_{Lmin} is computed as 0.81 at a Reynolds number of 100,000.

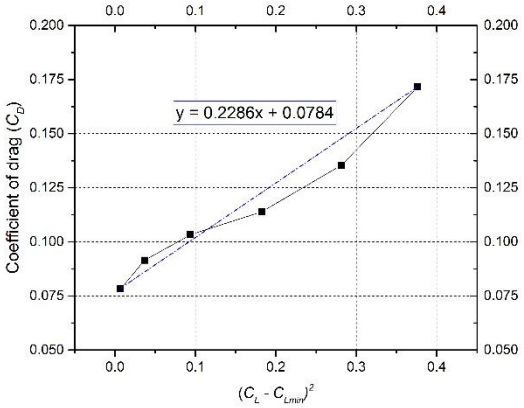

Figure 5: Viscous drag plot.

Finally, these values are substituted back into 3-D drag polar equation to obtain the airplane's 3D drag coefficient for all airfoil lift coefficients as shown in Figure 6.

International Journal of Emerging Technology and Advanced Engineering
Website: www.ijetae.com (ISSN 2250-2459, ISO 9001:2008 Certified Journal, Volume 7, Issue 8, August 2017)

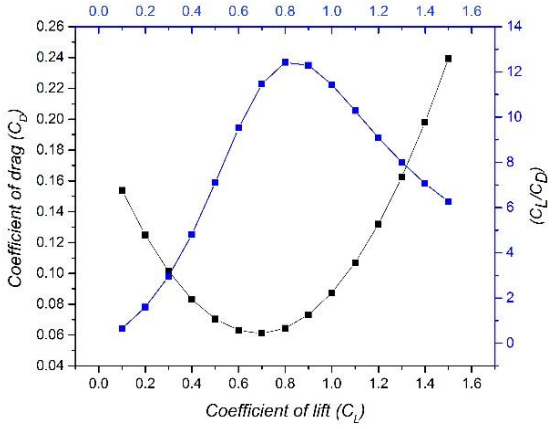

Figure 6: Drag polar of aircraft.

Figure 6 is the drag polar plot for the entire aircraft. For lift coefficient of 0.8, drag coefficient is 0.064 at which highest lift to drag ratio of 12.41 is obtained. The equation shown is used to determine the total resulting 3D drag for the airplane. The final drag polar equation is,

$$C_D = 0.0382 + 0.042C_L^2 + 0.2286(C_L - 0.81)^2$$

IV. Stability & Control

The ability of the plane to come back to equilibrium is termed stability and the influence that the controller can exert on equilibrium is known as controllability. The magnitude of restoring forces depends on relative position of neutral point with respect to centre of gravity. The position of neutral point is governed by the area of the tail and the length of the moment arm as shown in Figure 7.

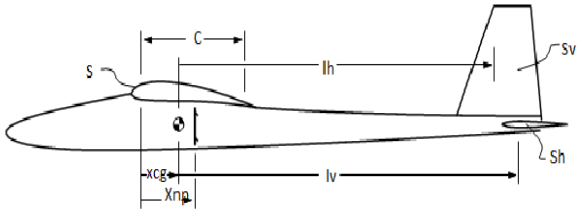

Figure 7: Position of COG & its effect on stability [4].

The static margin is the distance between neutral point and centre of gravity. The centre of gravity must lie ahead of the neutral point for positive stability. If the centre of gravity is behind the neutral point, the aircraft is longitudinally unstable .This concept is used to find the neutral point and also tail sizing.

Dynamic stability causes the plane to arrive at original position after a series of damped oscillations. A small change in the angle of attack changes the moment coefficient which in turn brings the plane back to original configuration. Static Margin is given by

$$SM(\%) = \frac{X_{NP} - X_{CG}}{MAC} \text{ x } 100$$

For empty weight, the centre of gravity of aircraft is located at 25% of Mean Aerodynamic Chord (MAC) which is 3.75cm from leading edge. The neutral point of the plane is located at 38% of MAC which is 5.63cm from leading edge. Therefore static margin for unloaded case is 12.5%. When the aircraft carries payload, the position of centre of gravity is present at 30% MAC. Therefore Static Margin for loaded case is 7.5%. Thus the airplane has significant amount of stability both in loaded and unloaded case.

V. Wing Structure Analysis

Wing is the most essential component of an aircraft. The structural analysis of the wing is done using ANSYS static structural workbench. The wing is considered as a cantilever beam subjected to various types of loading. Here the load on the wing is the lift force. The material of the wing is Balsa wood. The wing structure is analyzed for 1g and 2g conditions. At cruise conditions, the weight of airplane balances the lift generated by wing. Therefore the load acting on the wing is equal to the weight of aircraft. This is 1g condition. The load acting on one particular wing is 0.75kg.

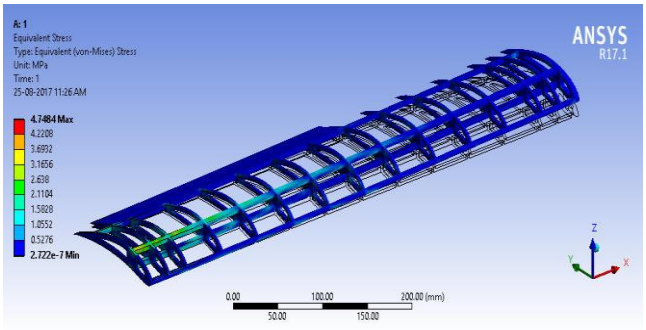

Figure 8: Stress analysis for 1g condition.

The stress developed on the wing frame for 1g condition is as shown in Figure 8. The ribs at one end is fixed. The load considered is acting at the center of pressure of the wing. The maximum stress achieved at 1g condition is 4.74Mpa. The yield strength of balsa wood is 15Mpa.

International Journal of Emerging Technology and Advanced Engineering
Website: www.ijetae.com (ISSN 2250-2459, ISO 9001:2008 Certified Journal, Volume 7, Issue 8, August 2017)

Therefore a FOS of 3.2 is present which is within the limits. The maximum deformation observed at 1g condition is 0.19mm.

When the aircraft rolls, the load acting on the wing will increase. Therefore the wing is also analyzed for higher loads to check the structural integrity. The wing is analyzed for 2g condition. The load acting on one particular wing is 1.5kg.

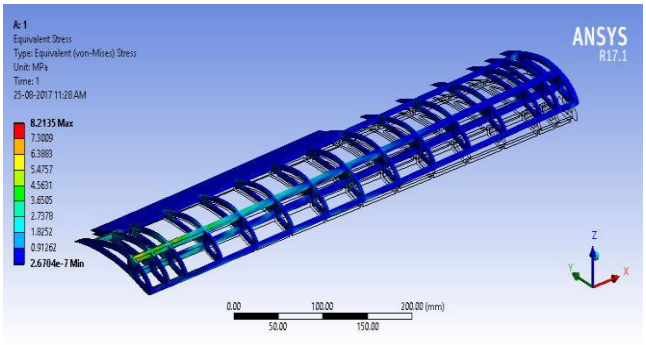

Figure 9: Stress analysis for 2g condition.

The maximum deformation observed at 2g condition is 0.80mm.The maximum stress induced in the wing for 2g loading condition is 8.21Mpa as shown in Figure 9. Therefore a FOS of 1.83 is present which is within the limits.

VI. CFD Analysis

CFD analysis of airfoil E423 is carried out using the analysis software ANSYS. ICEM is used to obtain the mesh. As shown in the figure mapped mesh of C-grid type is used and y^+ value of 0.9 is maintained to capture the results at the boundary layer of the airfoil. The grid size normal to the airfoil is 1.8e-5 as shown in Figure 10.

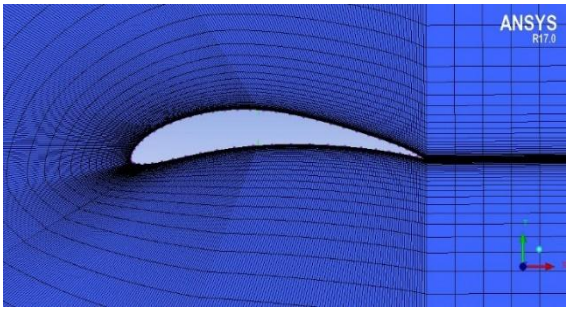

Figure 10: C-grid mesh.

K-omega SST is used as the turbulence model to simulate the flow around airfoil [6]. The simulation is carried out for a Reynolds number of 100,000 which corresponds to a velocity of 10m/s for a chord of 0.15m.

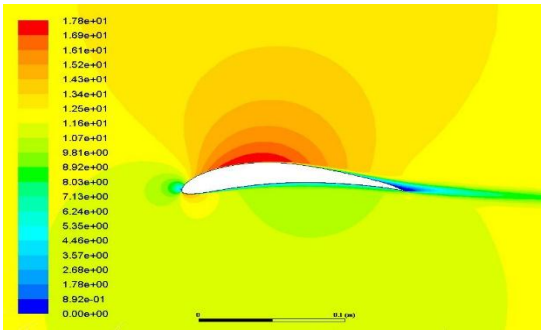

Figure 11: Velocity contour for airfoil E423.

From the velocity contour as shown in Figure 11, the maximum velocity achieved at the top of airfoil is 17.8m/s. This is the region where static pressure is minimum. The pressure distribution around the airfoil is given by static pressure plot as shown in Figure 12.

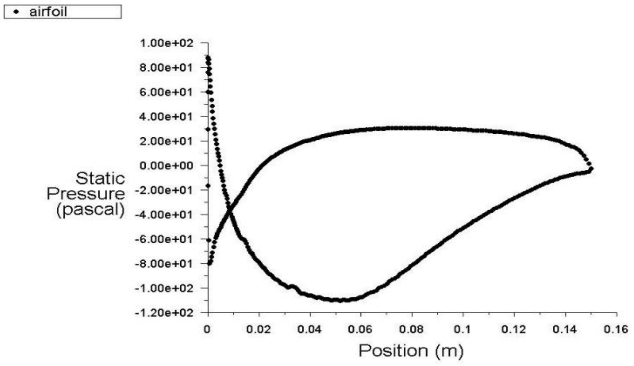

Figure 12: Static pressure variation over airfoil.

VII. Manufacturing

Balsa wood was primarily used for building the aircraft because of its light weight and high strength to weight ratio. Different manufacturing processes & methods are considered and qualitatively compared to the built-up balsa technique. After conducting extensive literature survey on different materials it is found that birch wood pad is perfect for mounting the motor to the fuselage due to its high strength and rigidity which reduces the inherent vibrations of the motor.

A. Wing

The wing of the plane is manufactured using balsa wood and is ultimately wrapped with ultrakote. Balsa wood is light and strong at the same time and is also capable of carrying a very heavy payload. Weight of wing structure is reduced by making it hollow.

The hollow structure is achieved by aligning pieces of balsa wood in the shape of airfoil over which ultrakote is wrapped. Truss structure is used in order to increase the strength of the wing.

B. Fuselage

The fuselage of the plane is made rectangular in design with slight taper at the rear of the plane for manufacturing easement and to reduce weight. The fuselage is wide enough to incorporate all the electronic components inside the plane. The payload bay has the space to shift inside the fuselage to maintain the position of centre of gravity from low payload to high payload ratio. The positions of all the components is in the front and they are placed considering the centre of gravity of the plane before and after the payloads are secured. The wing is secured to the plane by employing a bolt and nut and using birch wood pad. Additional wood padding is provided to secure the wing to the fuselage at the side.

C. Tail

After doing a figure of merit study of various tail configurations the team decided to adopt conventional design. The pad of stabilizer and the vertical tail is made of balsa wood which can sustain lift generated by the stabilizer for pitching and also the movement of vertical tail. The balsa wood is laser cut to thin flat sheet with internal truss structure which significantly reduces the weight of airplane. The thin balsa sheet further reduces drag and proves to be more efficient for a stable flight.

Figure 13: Final prototype plane

REFERENCES

[1] John J.Bertin, Russell M.Cummings, Aerodynamics for Engineers, International Edition 6, Pearson Education Limited, ISBN 0273793527, 2013, 832 pages.

[2] UIUC Airfoil coordinate database. URL http://m-selig.ae.illinois.edu/ads/coord_database.html.

[3] Anderson, J., Fundamentals of Aerodynamics. McGraw-Hill Education, 2010. ISBN 9780073398105. URL https://books.google.co.in/books?id= xwY8PgAACAAJ.

[4] Control & Stability. URL https://surjeetyadav.wordpress.com/author/surjeetyadav/page/2/Anderson.

[5] Aircraft performance and design. McGraw-Hill Education. ISBN 0070702454, 9780070702455. URL https://books.google.co.in/books/about/Aircraft_Performance_Design.html?id=Ck9l1DGj5-4C&redir_esc=y.

[6] Wilcox, David C (1998). "Turbulence Modeling for CFD". Second edition. Anaheim: DCW Industries, 1998. pp. 174.

[7] Selig, Michael S. "High-Lift Low Reynolds Number Airfoil Design". Published in Journal of Aircraft, Vol. 34, No. 1, January-February 1997.